GEOPHYSICS, VOL. 69, NO. 5 (SEPTEMBER-OCTOBER 2004); P. 1299–1310, 16 FIGS., 1 TABLE.
10.1190/1.1801946

Controlling amplitudes in 2.5D common-shot migration to zero offset

Jörg Schleicher[1] and Claudio Bagaini[2]

ABSTRACT

Configuration transform operations such as dip moveout, migration to zero offset, and shot and offset continuation use seismic data recorded with a certain measurement configuration to simulate data as if recorded with other configurations. Common-shot migration to zero offset (CS-MZO), analyzed in this paper, transforms a common-shot section into a zero-offset section. It can be realized as a Kirchhoff-type stacking operation for 3D wave propagation in a 2D laterally inhomogeneous medium. By application of suitable weight functions, amplitudes of the data are either preserved or transformed by replacing the geometrical-spreading factor of the input reflections by the correct one of the output zero-offset reflections. The necessary weight function can be computed via 2D dynamic ray tracing in a given macrovelocity model without any a priori knowledge regarding the dip or curvature of the reflectors. We derive the general expression of the weight function in the general 2.5D situation and specify its form for the particular case of constant velocity. A numerical example validates this expression and highlights the differences between amplitude preserving and true-amplitude CS-MZO.

INTRODUCTION

Configuration transforms like dip-moveout correction (DMO), migration to zero offset (MZO), shot or offset continuation (SCO and OCO, respectively), and azimuth-moveout correction (AMO) have become a field of great interest in exploration seismics. The objective of a configuration transform is to simulate a seismic section as if obtained with a certain measurement configuration but using the data recorded with another configuration. This type of imaging process is not only useful in the seismic processing chain for an improved stack (i.e., for data reduction and signal-to-noise enhancement), but also for wave-equation–based trace interpolation to reconstruct missing data and for velocity analysis. There are quite a number of publications in the area that demonstrate the use of configuration transforms for these purposes, for example, on MZO and DMO in the common-offset domain[1] (Black et al., 1993; Bleistein and Cohen, 1995; Canning and Gardner, 1996; Collins, 1997; Tygel et al., 1998; Bleistein et al., 1999) or in the common-shot domain (Biondi and Ronen, 1987), OCO (Fomel, 1994, 2003; Santos et al., 1997; Fomel and Bleistein, 2001) SCO (Bagaini and Spagnolini, 1996), and AMO (Biondi et al., 1998).

In this paper, we investigate another of these configuration transform methods: common-shot migration to zero offset (CS-MZO). Its purpose is to transform a single common-shot section into a zero-offset section. This can be realized as a direct one-step procedure or split up into two steps: a normal moveout (NMO) plus a subsequent common-shot DMO (CS-DMO). The kinematic properties of the latter process have already been studied by Biondi and Ronen (1987), who also proposed a cost-effective implementation in the log-stretch domain. To further reduce the method's computation time, Cabrera and Levy (1989) and Granser (1994) suggested approximate versions of the CS-DMO operator. Hearn (1989) pointed out the importance of controlling the weights for a space-time implementation of CS-DMO and, based on a geometrical analysis, suggested a first amplitude distribution. Here, we derive the correct weights for Kirchhoff CS-MZO.

The advantage of the common-shot implementation over the standard one in the common-offset domain is that no data sorting is needed. Moreover, a CS-MZO simulated zero-offset section is obtained from a different subset of the data than a standard one. Therefore, it not only provides a different illumination of the subsurface region and suffers from different boundary effects, but it also enables an independent quality control over the velocity information used in the procedure.

[1]MZO is defined in homogeneous media as the cascade of NMO and DMO. In inhomogeneous media, MZO is a more general process that can be split only approximately into NMO and DMO.

Manuscript received by the Editor September 30, 2003; revised manuscript received March 1, 2004.
[1]State University of Campinas, IMECC, Department of Applied Mathematics, CP 6050, 13083-970, Campinas, São Paulo, Brazil. E-mail: js@ime.unicamp.br.
[2]Schlumberger Middle East S.A., Schlumberger Dhahran Carbonate Research Center, P.O. Box 2836, Al-Khobar 31952, Saudi Arabia. E-mail: bagaini@dhahran.oilfield.slb.com.

Here, we discuss the realization of a CS-MZO in form of a Kirchhoff-type stacking operation. Moreover, we address particular features of CS-MZO such as how to control the simulated zero-offset amplitudes by an adequate weight in the Kirchhoff implementation and how to choose the correct operator aperture.

There are two main competing concepts in the seismic imaging literature that receive the designations "amplitude preserving" or "true amplitude." In this paper, we adopt the term "true amplitude" for imaging procedures that treat the input amplitudes in such a way that the geometrical-spreading factors are correctly transformed. We reserve the term "amplitude preserving" for procedures that do not alter the input amplitudes.

From the "amplitude-preserving" point of view, Black et al. (1993) showed that, for a constant-velocity medium, the standard multistep imaging sequence consisting of spherical-divergence correction, NMO, DMO, and zero-offset migration yields an image with peak amplitudes that are proportional to angle-dependent reflection coefficients if the DMO step is amplitude preserving. An essential assumption in Black et al.'s way of achieving an amplitude-preserving DMO is that the seismic data are collected over a reflector whose radius of curvature is infinite, (i.e., a dipping planar reflector). For curved reflectors, Black et al.'s DMO does not preserve amplitudes because any DMO includes an inherent curvature-related amplitude modification (Tygel et al., 1998).

From the "true-amplitude" point of view, Tygel et al. (1996) demonstrated that any configuration transform method can be realized as a Kirchhoff procedure. Moreover, such a procedure automatically transforms the curvature-dependent part of the geometrical-spreading factor from the input to the output configuration, independently of the chosen weight function. As long as a curvature independent weight is used—and such a weight must always be used because the reflector curvature is a priori unknown—the resulting peak amplitudes after CS-MZO will be inversely proportional to the curvature term of the zero-offset geometrical-spreading factor.

Based on this general observation, Tygel et al. (1998) overcame the planar-reflector assumption for the common-offset MZO operator. In their work, they establish the true-amplitude (i.e., geometrical-spreading-correct) weight function for integral MZO regardless of the reflector curvature. The corresponding formulas for constant-velocity media were derived by Fomel and Bleistein (2001). With this weight function, an MZO applied to common-offset data without spherical-divergence correction simulates zero-offset amplitudes that are proportional to the ratio between the (angle- and offset-dependent) reflection coefficient and the zero-offset spreading factor. To obtain spreading-free amplitudes in the zero-offset sections [e.g., to carry out an amplitude-variation-with-offset (AVO) or amplitude-variation-with-angle (AVA) analysis in time domain], the spherical-divergence correction is applied after MZO.

However, the multistep imaging sequence that yields a migrated true-amplitude image requires no spherical-divergence correction at all to be applied. It consists of true-amplitude MZO (possibly split into NMO plus DMO) and a subsequent zero-offset migration [also with curvature-independent weights, see Hubral et al. (1991)]. The spherical-divergence correction is taken care of by the curvature-independent weights of MZO and migration.

From the above considerations, it becomes clear that the true-amplitude approach is more fundamental. With only curvature-independent weights, the whole processing sequence can be followed to end up with reflection amplitudes that are correctly freed of their geometrical spreading. The amplitude-preserving approach, on the other hand, cannot be curvature independent because it necessarily includes a spherical-divergence correction to be applied somewhere in the processing sequence. For this reason, amplitude-preserving approaches (see, e.g., Black et al., 1993) assume planar reflectors.

In this work, we discuss CS-MZO weights for both types of amplitude processing. With true-amplitude weights, the CS-MZO procedure proposed here is designed to produce, from a common-shot section, a simulated zero-offset section that is kinematically and dynamically equivalent to the one obtained from common-offset data using a true-amplitude MZO. In other words, the true-amplitude weight function for CS-MZO acts so that the simulated zero-offset amplitudes are proportional to the ratio between the original angle-dependent common-shot reflection coefficient and the zero-offset geometrical-spreading factor. In this way, these amplitudes are directly comparable to those obtained from a true-amplitude MZO or from modeling a synthetic zero-offset section. On the other hand, with amplitude-preserving weights, spherical-divergence corrected common-shot sections can be transformed to corresponding zero-offset sections so as to directly enable an AVO or AVA analysis in the time domain.

KIRCHHOFF-TYPE CS-MZO

Like conventional MZO in the common-offset domain, CS-MZO also is based on the general 3D Kirchhoff-type formula for configuration transforms of Tygel et al. (1996), who discuss a unified approach to true-amplitude seismic reflection imaging for 3D seismic records with arbitrary measurement configurations and laterally and vertically inhomogeneous, isotropic macrovelocity models. Here, we consider a 2.5D situation, that is, 3D wave propagation in a 2D (isotropic, vertically and laterally inhomogeneous) earth model. No medium variations exist in the out-of-plane y-direction perpendicular to the seismic line. In particular, all reflectors can be specified by in-plane (x, z)-curves. Moreover, all point sources, assumed to omnidirectionally emit identical pulses, and all receivers, assumed to have identical characteristics, are distributed along the x-axis so that only in-plane propagation needs to be considered. For the 2.5D problem, the full 3D geometrical-spreading factor of an in-plane ray can be written as product of in-plane and out-of-plane factors (Bleistein, 1986). Both quantities can be computed using 2D dynamic ray tracing (Červený, 1987).

Let the original (input) common-shot measurement configuration be parameterized by the (fixed) source coordinate s and the (variable) half-offset coordinate h (see Figure 1; Table 1). On the measurement surface $z = 0$ and along the seismic line $y = 0$, these coordinates define the locations of the fixed source at $S = (s, 0, 0)$ and the corresponding receivers at $G = G(h) = (s + 2h, 0, 0)$. At each receiver position G, a scalar wavefield induced by the corresponding point source at S is recorded. The output zero-offset configuration is parametrized by the coordinate s_0 that describes coincident source-receiver pairs at $S_0(s_0) = G_0(s_0) = (s_0, 0, 0)$.

In the following, we assume that each (real) seismic trace in the input section has already been transformed into its corresponding analytic (complex) trace by adding the Hilbert transform of the original trace as the imaginary part. (As for other Kirchhoff procedures, the analytic traces are needed to account for caustics along the ray path and to correctly recover complex reflection coefficients.) Therefore, the output common-offset section will be also considered analytic. The analytic traces of the input section are denoted by $U(h, t)$, where t is the time coordinate of the common-shot section. Correspondingly, the analytic traces of the output section are denoted by $U_0(s_0, t_0)$, where t_0 is the time coordinate of the simulated zero-offset section.

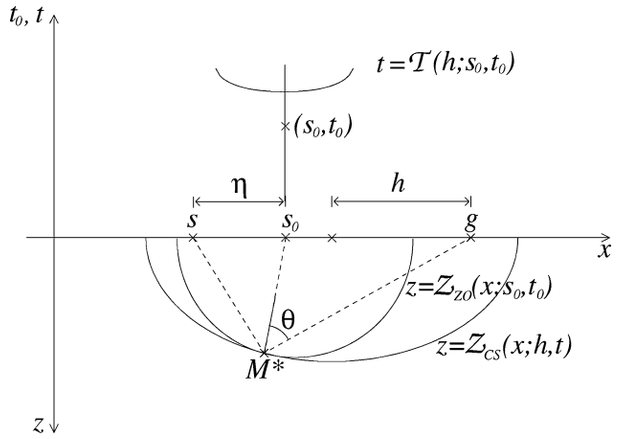

Figure 1. Geometrical properties of a common-shot MZO. Depicted are the common-shot and zero-offset isochrons $z = \mathcal{Z}_{CS}$ and $z = \mathcal{Z}_{ZO}$. Their tangency point M^* defines the CS-MZO stacking line $\mathcal{T}$ as a function of half-offset h for a given point (s_0, t_0).

Stacking integral

For each point (s_0, t_0) in the output zero-offset section to be simulated, the stack result $U_0(s_0, t_0)$ will be obtained by means of a weighted stack of the input data, represented by

$$U_0(s_0, t_0) = \frac{1}{\sqrt{2\pi}} \int_A dh \mathcal{W}(h; s_0, t_0) \times D_-^{1/2}[U(h, t)]\big|_{t=\mathcal{T}(h;s_0,t_0)}. \quad (1)$$

Similar to the situation in other familiar 2.5D Kirchhoff-type imaging procedures such as migration (Bleistein et al., 1987; Martins et al., 1997), DMO (Black et al., 1993), OCO (Santos et al., 1997), or MZO (Tygel et al., 1998), the input traces $U(h, t)$ are weighted by a certain factor $\mathcal{W}(h; s_0, t_0)$ and then summed up along the stacking line $t = \mathcal{T}(h; s_0, t_0)$. Both functions depend on the point (s_0, t_0) where the stack is to be placed, as well as on the variable h that specifies the traces being considered in the stack. Moreover, A denotes the aperture of the stack (i.e., the range of half-offsets for which data are available in the input section). Finally, the (time-reverse) time half-derivative, given by

$$D_-^{1/2}[f(t)] = \mathcal{F}^{-1}\left[|\omega|^{1/2} e^{-i\frac{\pi}{4}\mathrm{sign}(\omega)} \mathcal{F}[f(t)]\right], \quad (2)$$

where $\mathcal{F}$ denotes the Fourier transform, is needed to correct the pulse shape. It is a natural 2.5D counterpart (Bleistein et al.,

Table 1. Glossary.

MZO	migration to zero offset (i.e., seismic imaging process that transforms a common-offset section into a simulated zero-offset section)
DMO	dip moveout correction (i.e., seismic imaging process that transforms an NMO-corrected common-offset section into a simulated zero-offset section)
CS-MZO	common-shot MZO
CS-DMO	common-shot DMO
s, h, t	shot position, half offset, and time coordinate in original common-shot section
t_n	time coordinate in NMO-corrected common-shot section
s_0, t_0	location and time coordinate in zero-offset section to be constructed
η	shot shift $s_0 - s$ between reflections from the same reflection point in shot- and zero-offset sections
(S, G)	source-receiver pair in the common-shot configuration
(S_0, G_0)	source-receiver pair in the zero-offset configuration, $G_0 \equiv S_0$
$U(h, t)$	original common-shot seismograms (analytic traces)
$U_0(s_0, t_0)$	simulated zero-offset seismograms (analytic traces) obtained by CS-MZO
h_B	2D Beylkin determinant
$\mathcal{T}$	stacking line for Kirchhoff CS-MZO for fixed s_0, t_0 and varying h
$\tilde{\mathcal{T}}$	stacking line for Kirchhoff CS-DMO
$\mathcal{W}^{TA}, \mathcal{W}^{AP}$	true-amplitude and amplitude-preserving weight functions for Kirchhoff CS-MZO
$\tilde{\mathcal{W}}^{TA}, \tilde{\mathcal{W}}^{AP}$	true-amplitude and amplitude-preserving weight functions for Kirchhoff CS-DMO
$D_-^{1/2}$	symbol for the time-reverse half derivative in time
A	CS-MZO aperture
$\mathcal{Z}_{ZO}$	zero-offset isochron for fixed (s_0, t_0) and varying x, defined by all points M for which the reflection traveltime from S_0 to $G_0 \equiv S_0$ equals t_0
$\mathcal{Z}_{CS}$	common-shot isochron for fixed (s, h, t) and varying x, defined by all points M for which the reflection traveltime from S to G equals t
M	arbitrary point in depth with coordinates (x, z)
M^*	tangency point of the common-shot and zero-offset isochrons $\mathcal{Z}_{CS}$ and $\mathcal{Z}_{ZO}$
K, K_0	in-plane curvatures of the common-shot and zero-offset isochrons $\mathcal{Z}_{CS}$ and $\mathcal{Z}_{ZO}$
v	wave velocity
θ	incident angle between the ray SM^* and the isochron normal at M^*

1987) to the full derivative that is part of a full 3D Kirchhoff-type migration scheme (Newman, 1975; Schleicher et al., 1993).

The stacking line $\mathcal{T}$ is defined by the kinematics of the operation, and the weight function $\mathcal{W}$ will be determined by the desired amplitude behavior. For the true-amplitude weight function, this is achieved by imposing the requirement that, asymptotically, the simulated reflections must have the same geometrical-spreading factor as corresponding true reflections in a zero-offset section. Correspondingly, for the amplitude-preserving weight, the imposed condition is that of unaltered amplitudes. As shown below, the resulting true-amplitude weight function does not depend on any reflector properties. It can be computed for any arbitrary point (s_0, t_0) in the zero-offset section to be simulated using no other information than that provided by the given smooth macrovelocity model.

Stacking line

Like any Kirchhoff operation, Kirchhoff CS-MZO can be realized as a stack over the input data along inplanats or a smear stack in the output domain along outplanats. Here, the terms inplanat and outplanat are used as defined by Hubral et al. (1996), that is, an inplanat is the kinematic image in the input section of a point in the output section and, correspondingly, an outplanat is the kinematic image in the output section of a point in the input section of the imaging operation under consideration. For example, in the case of migration, the inplanat is the diffraction-traveltime surface and the outplanat is the isochron.

To explain the construction of the stacking line or inplanat $\mathcal{T}$ of Kirchhoff CS-MZO (see also Figure 1 for the constant-velocity case), let us start from a fixed point (s_0, t_0) in the output section. The corresponding inplanat $\mathcal{T}(h; s_0, t_0)$ is then constructed by the following two-step procedure:

1) For the given point (s_0, t_0), determine the isochron in depth, $z = \mathcal{Z}_{ZO}(x; s_0, t_0)$. This isochron is implicitly defined by all depth points $M = (x, \mathcal{Z}_{ZO}(x; s_0, t_0))$ for which the sum of the traveltimes along the two ray segments S_0M and MG_0 connecting M to the source-receiver pair (S_0, G_0), equals the given time coordinate t_0, viz.,

$$\tau(S_0, M) + \tau(M, G_0) = 2\tau(S_0, M) = t_0. \qquad (3)$$

   These traveltimes $\tau(S_0, M)$ and $\tau(M, G_0)$ are to be constructed in the given macrovelocity model. For constant velocity, the resulting isochron is the lower half-circle with center at $S_0 = G_0$ and radius $R_0 = vt_0/2$.
2) Treat the isochron (equation 3) as a reflector and construct its reflection traveltime curve with the input configuration, that is, compute the reflection traveltimes for all source-receiver pairs (S, G) by forward modeling. The resulting CS-MZO stacking curve may then be written as

$$t = \mathcal{T}(h; s_0, t_0) = \tau(S, M^*) + \tau(M^*, G), \qquad (4)$$

   where, for each half-offset h, point M^* is the specular reflection point on the isochron $z = \mathcal{Z}_{ZO}(x; s_0, t_0)$ of the source-receiver pair (S, G) specified by h. Point M^*, which is assumed to be unique, has the coordinates $(x^*, \mathcal{Z}_{ZO}(x^*; s_0, t_0))$, where $x^* \equiv x^*(h; s_0, t_0)$ is obtained using the stationarity condition

$$\frac{\partial}{\partial x}(\tau(S_0, M) + \tau(M, G_0))|_{x=x^*} = 0. \qquad (5)$$

In the first section of Appendix A, the CS-MZO stacking line $t = \mathcal{T}(h; s_0, t_0)$ for a constant-velocity medium is actually constructed following the above geometrical prescriptions. It reads

$$\mathcal{T}(h; s_0, t_0) = \frac{2h}{v}\sqrt{1 + \frac{R_0^2}{\eta(2h - \eta)}}, \qquad (6)$$

where $\eta = s_0 - s$ is the distance between the common source point of the input section and the desired output point (see Figure 1). This stacking line or inplanat is, of course, equivalent to the smear-stacking ellipse or outplanat

$$\frac{(vt_0)^2}{(vt)^2 - (2h)^2} + \frac{(\eta - h)^2}{h^2} = 1 \qquad (7)$$

previously derived by Biondi and Ronen (1987) or Hearn (1989).

We see from equation 6 that a real stacking line exists only if $\eta \neq 0$, $\eta \neq 2h$, and $[R_0^2/\eta(\eta - 2h)] \leq 1$. The first conditions implies that we cannot construct a zero-offset trace at the source position. The second condition means that for the construction of the zero-offset trace at a distance of η from the source, the trace recorded at this position must not enter the stack. The requirement of a continuous and smooth stacking line together with the third condition already provides a first condition for the aperture A of stack 1. Certainly, only half-offsets $0 < h < \eta/2$ or $h > \eta/2$ will enter the stack. We see in the next section that the aperture actually needed is even smaller.

CS-MZO aperture

The basic condition for the aperture is the existence of the stationary point of integral 1. In other words, the aperture includes all receivers G for which a reflection point M^* on the zero-offset isochron as defined by equation 5 exists. In inhomogeneous media, where the stacking lines have to determined by the above procedure, the aperture is thus automatically determined. For constant velocity, this condition can be discussed analytically. This has been done in detail in Appendix A. It results in the following condition for h:

$$\begin{aligned} &\text{For} \quad \eta < R_0/2: \quad \frac{\eta(R_0 + \eta)}{R_0 + 2\eta} < h < \frac{\eta(R_0 - \eta)}{R_0 - 2\eta}. \\ &\text{For} \quad \eta \geq R_0/2: \quad \frac{\eta(R_0 + \eta)}{R_0 + 2\eta} < h. \end{aligned} \qquad (8)$$

Note that the left-hand side expression in inequality 8 is always larger than $\eta/2$ but smaller than η. The alternative condition that the maximum time dip must not exceed $1/v$ yields the same aperture condition 8.

Condition 8 means that for large η (i.e., zero-offset traces far away from the source), an infinite offset is needed, whereas for small η (i.e., zero-offset traces relatively close to the source position), the stack 1 is carried out over a finite aperture. It

is important to note that the CS-MZO aperture may even reduce to very few traces, thus becoming insufficient. As a Kirchhoff operation, CS-MZO needs sufficient traces to guarantee interference in the stack 1. Where this cannot be achieved (i.e., where too few tangency points between the common-offset and zero-offset isochrons exist), we can say that these two isochrons are practically undistinguishable. There, the aperture should be reduced to include only the one single trace at the center of the zero-offset isochron (i.e., at $h=\eta$) to be used without a weight and without the half-derivative operation.

Weight function

Analogously to the above, we now consider the isochron of a point (h,t) in the input section, this isochron is assumed to exist and is parameterized in the form $z=\mathcal{Z}_{CS}(x;h,t)$. For constant velocity, this is the lower half-ellipse with foci at S and G and semiaxes $a=vt/2$ and $b=\sqrt{a^2-h^2}$. The isochron $z=\mathcal{Z}_{CS}(x;h,t)$ is tangent to the isochron $z=\mathcal{Z}_{ZO}(x;s_0,t_0)$ at M^* for arbitrarily heterogeneous macrovelocity models.

Let us now denote the 3D point-source geometrical spreading factors for the ray segments SM^* and M^*G by $\mathcal{L}_S$ and $\mathcal{L}_G$, respectively. Correspondingly, we denote the 3D point-source geometrical spreading factors for the ray segments S_0M^* and M^*G_0 by $\mathcal{L}_0$. Moreover, let the velocity at M^* be denoted by v^*, and let θ denote the incident angle between the ray SM^* and the isochron normal at M^*. Note that this is half the angle between the ray segments SM^* and M^*G. We also need the in-plane curvatures K and K_0 of the isochrons $z=\mathcal{Z}_{CS}(x;h,t)$ and $z=\mathcal{Z}_{ZO}(x;s_0,t_0)$, respectively, at M^*. In homogeneous media, the latter is a circle with curvature $K_0=-1/R_0$ (see Figure 1). Furthermore, the out-of-plane Fresnel geometrical-spreading factors (Tygel et al., 1994) of the rays SMG and S_0MG_0 are denoted by $\mathcal{L}_F$ and $\mathcal{L}_{F0}$, respectively. Finally, let h_B be the 2D Beylkin determinant (Beylkin, 1985; Bleistein, 1987; Tygel et al., 1995). With the help of these quantities, the true-amplitude weight function $\mathcal{W}^{TA}(h;s_0,t_0)$ can be expressed as

$$\mathcal{W}^{TA}(h;s_0,t_0)=\left(\frac{v^*}{2}\right)^{3/2}\frac{\mathcal{L}_S\mathcal{L}_G}{\mathcal{L}_0^2}\frac{\mathcal{L}_{F0}}{\mathcal{L}_F}\frac{1}{\cos^2\theta}\frac{|h_B|}{\sqrt{|K-K_0|}}\times\exp\left\{i\frac{\pi}{2}\kappa\right\},\tag{9}$$

where $\kappa=(1-\mathrm{sign}(K-K_0))/2$. The derivation of expression 9 is virtually identical to that of the true-amplitude weight function for common-offset MZO (see Tygel et al., 1998, their Appendix A) and need not be repeated here.

We remind the reader that, because we are considering the 2.5D situation, any of the 3D geometrical-spreading factors $\mathcal{L}$ can be computed as the product of the corresponding 2D factor $\tilde{\mathcal{L}}$ and the out-of-plane spreading given by the integral $\sigma=\int v^2 d\tau$ along the ray. With the expression of Tygel et al. (1994) for the out-of-plane Fresnel geometrical-spreading factor,

$$\mathcal{L}_F=\left(\frac{1}{\sigma_S}+\frac{1}{\sigma_G}\right)^{-1/2},\tag{10}$$

the weight function 9 can be completely expressed in terms of 2D quantities as

$$\mathcal{W}^{TA}(h;s_0,t_0)=\left(\frac{v^*}{2}\right)^{3/2}\frac{\tilde{\mathcal{L}}_S\tilde{\mathcal{L}}_G}{\tilde{\mathcal{L}}_0^2}\sqrt{\frac{\sigma_S+\sigma_G}{2\sigma_0}}\times\frac{1}{\cos^2\theta}\frac{|h_B|}{\sqrt{|K-K_0|}}\exp\left\{i\frac{\pi}{2}\kappa\right\}.\tag{11}$$

Since a CS-MZO using the true-amplitude weight function replaces the original 3D geometrical-spreading factor $\mathcal{L}$ in the data by the zero-offset geometrical-spreading factor $\mathcal{L}_0$, the theoretical amplitude-preserving weight function can be obtained from the above expressions by scaling them with the ratio $\mathcal{L}_0/\mathcal{L}$. These factors are, however, curvature dependent and thus generally unknown. Under the planar-reflector assumption, their ratio can be replaced by the ratio of the traveltimes, τ_0/τ. Note that this factor transforms the approximate geometical-spreading correction by traveltime scaling from the common-shot to the zero-offset domain. The error for a curved reflector is the same as discussed in detail by Tygel et al. (1998) for common-offset MZO.

As shown in Appendix A, the true-amplitude CS-MZO weight function 9 reduces for a constant velocity v to

$$\mathcal{W}^{TA}(h;s_0,t_0)=\sqrt{\mathcal{T}}\sqrt{\frac{\eta}{(2h-\eta)^3}},\tag{12}$$

where $\mathcal{T}$ is given by equation 6. For an amplitude-preserving CS-MZO (i.e., one that does not alter peak amplitudes of reflections from planar reflectors), the weight function is

$$\mathcal{W}^{AP}(h;s_0,t_0)=\frac{t_0}{\sqrt{\mathcal{T}}}\sqrt{\frac{\eta}{(2h-\eta)^3}},\tag{13}$$

which is obtained from equation 12 by scaling it with $t_0/\mathcal{T}$. Here, we have made use of the fact that (1) the traveltime of the zero-offset event to be simulated at t_0 is given by $\tau_0=t_0$, and (2) at the stationary point, the traveltime of the common-shot event that gives rise to this simulated event is $\tau=\mathcal{T}$.

If the CS-MZO operation 1 is applied to a NMO-corrected common-shot section (i.e., as a common-shot DMO), the stacking line and the weight function must be modified. The CS-DMO stacking line is obtained from an NMO correction of the CS-MZO stacking line,

$$t_n=\widetilde{\mathcal{T}}(h,s_0,t_0)=\sqrt{\mathcal{T}^2-4h^2/v^2}=\frac{t_0\,h}{\sqrt{\eta(2h-\eta)}},\tag{14}$$

where t_n is the time coordinate of the NMO-corrected common-shot section. Because of the properties of fractional derivatives, the weight functions are transformed by multiplying them with $[\partial\widetilde{\mathcal{T}}/\partial t]^{1/2}=[\mathcal{T}/\widetilde{\mathcal{T}}]^{1/2}$. Thus, the true-amplitude CS-DMO weight function is

$$\widetilde{\mathcal{W}}^{TA}(h;s_0,t_0)=\frac{\sqrt{\widetilde{\mathcal{T}}^2+4h^2/v^2}}{\sqrt{\widetilde{\mathcal{T}}}}\sqrt{\frac{\eta}{(2h-\eta)^3}}=\frac{\sqrt{\widetilde{\mathcal{T}}^2+4h^2/v^2}}{t_0}\sqrt{\widetilde{\mathcal{T}}}\frac{\eta}{h(2h-\eta)},\tag{15}$$

and the one for an amplitude-preserving CS-DMO is

$$\widetilde{\mathcal{W}}^{AP}(h; s_0, t_0) = \sqrt{\widetilde{\mathcal{T}}}\frac{\eta}{h(2h-\eta)}. \qquad (16)$$

Note that these weight functions are to be used if the half derivative in the CS-DMO is applied with respect to the NMO-corrected traveltime t_n. In many practical implementations of DMO, however, this derivative is taken with respect to the output zero-offset traveltime t_0. In this case, the above weight functions need to be slightly modified. Again, the rules for fractional derivatives require the scaling of the weight functions by $[\partial\widetilde{\mathcal{T}}/\partial t_0]^{-1/2} = [t_0/\widetilde{\mathcal{T}}]^{1/2}$. Then, the true-amplitude CS-DMO weight function is

$$\widetilde{\mathcal{W}}_0^{TA}(h; s_0, t_0) = \frac{\sqrt{\widetilde{\mathcal{T}}^2 + 4h^2/v^2}}{\sqrt{t_0}}\frac{\eta}{h(2h-\eta)}, \qquad (17)$$

which is identical to the expression given in equation 47 of Goldin and Fomel (1995) with $q = 0$. Correspondingly, the amplitude-preserving CS-DMO weight function is

$$\widetilde{\mathcal{W}}_0^{AP}(h; s_0, t_0) = \sqrt{t_0}\frac{\eta}{h(2h-\eta)}. \qquad (18)$$

The weight function of equation 18 is the CS-DMO equivalent to the one of Black et al. (1993) for a standard common-offset DMO.

Comparison to Hearn's weight

Based on a geometrically appealing discussion of amplitudes, Hearn (1989) suggested an amplitude-preserving CS-DMO weight function. However, a simple dimension analysis shows that it cannot be correct. Here, we compare it numerically to the above expressions. For that purpose, we rewrite it in our notation. With the help of the formulas in Appendix A, Hearn's weight can be represented as

$$\tilde{\mathcal{W}}_H^{AP} = \sqrt{\frac{\left(2R_0^2(1+\rho) - h^2\rho^2\right)\left(R_0^2(1+\rho) - h^2\rho^2\right)}{2R_0\left(R_0^2 + h^2 - (h-\eta)^2\right)^3}}, \qquad (19)$$

where ρ is given by equation A-8.

NUMERICAL EXPERIMENT

To verify the validity of the CS-MZO weight function 9, we use a simple synthetic example. The model (Figure 2) consists of two homogeneous acoustic half-spaces separated by a smoothly curved interface. The velocities above and below the interface are 3 and 3.5 km/s, respectively. For this model, we have simulated by ray tracing a common-shot experiment with 396 receivers, the first being located at an offset of 100 m from the source. Receiver spacing was 20 m, and the time sampling interval was 2 ms. The obtained common shot gather is represented in Figure 3, in which every seventh trace is shown.

To test our analytic results, we have applied the CS-MZO with the proposed weights to the modeled common-shot data. The resulting simulated zero-offset sections are depicted in Figures 4–6. Figure 4 shows the result of a CS-MZO using the true-amplitude weight 12. Figure 5 shows the result of a CS-MZO using the amplitude-preserving weight 13. Of course, prior to the application of the latter, the data of Figure 3 have been

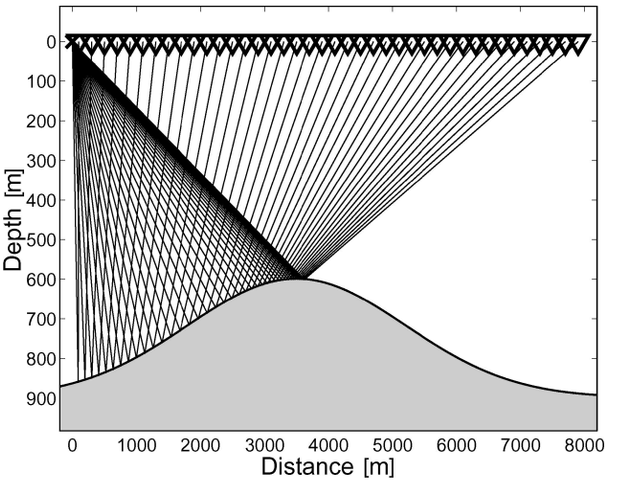

Figure 2. Earth model for the numerical experiment. Also shown is the ray family for the modeled common-shot experiment.

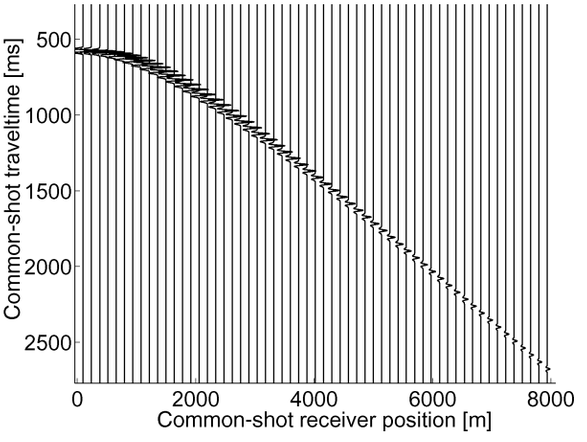

Figure 3. Ray-synthetic common-shot data for the numerical experiment.

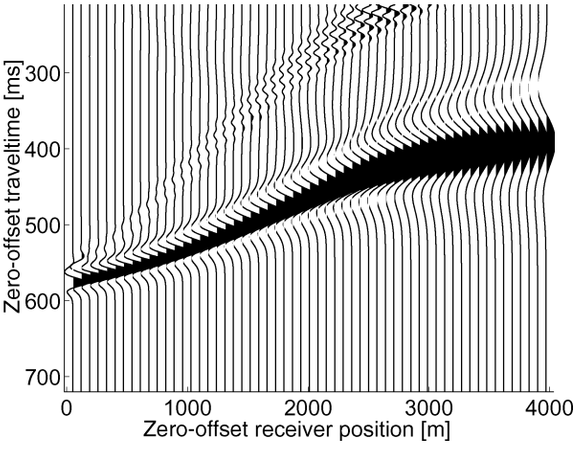

Figure 4. Result of a CS-MZO with true-amplitude weights applied to the data of Figure 3.

scaled by vt. For comparison, Figure 6 shows the result of a CS-MZO using a unit weight.

The quality of the obtained results can be checked best by a comparison to a modeled zero-offset section. Therefore, we have also simulated by ray tracing a zero-offset experiment with 396 receivers, equally spaced at every 10 m, beginning at 50 m from the original source. The resulting modeled zero-offset section is depicted in Figure 7. For better comparison between the amplitudes of the simulated and modeled common-offset sections, we refrained from using the correct angle-dependent reflection coefficient in the modeling but computed the common-offset and zero-offset reflections with a constant unit reflection coefficient. In this way, the simulated common-offset amplitudes after a true-amplitude CS-MZO should ideally be identical to those obtained from modeling.

Visual inspection of the simulated and modeled zero-offset sections permits some preliminary qualitative observations. The first impression of the simulated zero-offset sections of Figures 4–6 is mainly influenced by the strongly varying pulse length along the reflection event. This is due to the well-known fact that independently of any possible weights, configuration transformations do not reproduce the bandwidth of the modeled data. Like in the case of common-offset MZO (Tygel et al., 1998; Fomel and Bleistein, 2001), the pulse stretch is given by the cosine of the reflection angle.

Apart from the stretch effect, the general impression of the simulated zero-offset reflections is more or less the same in all figures. The shapes of all three simulated zero-offset reflections closely resemble the modeled one. The major differences lie in the different forms of the operator edge effects in the weighted and unweighted sections. While the unweighted CS-MZO has produced a strong "CS-MZO smile" (see Figure 6), the weighted CS-MZOs present a much weaker effect in the form of a dipping precursor to the simulated reflections (see Figures 4 and 5).

To enable a more quantitative analysis, the traveltimes and peak amplitudes along the simulated and modeled zero-offset reflections have been picked. The traveltimes are depicted in Figure 8. We see that the kinematic properties of the suggested

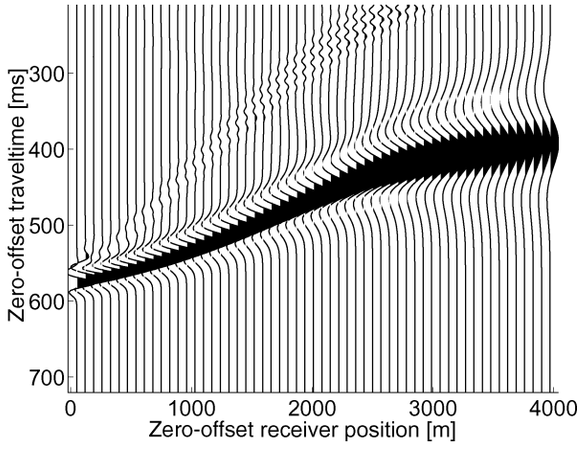

Figure 5. Result of a CS-MZO with amplitude preserving weights applied to the data of Figure 3 after time scaling.

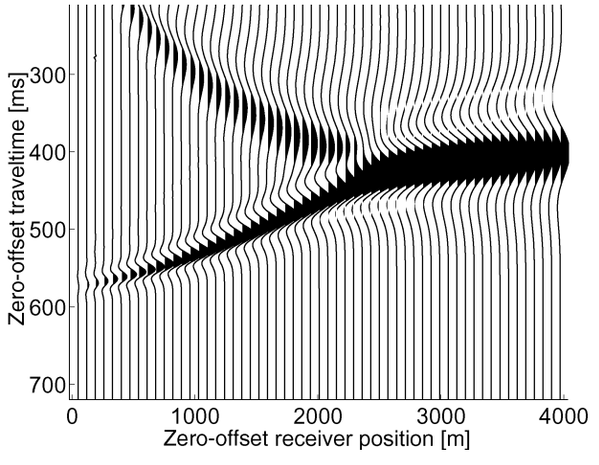

Figure 6. Result of a CS-MZO with no (i.e., unit) weights applied to the data of Figure 3.

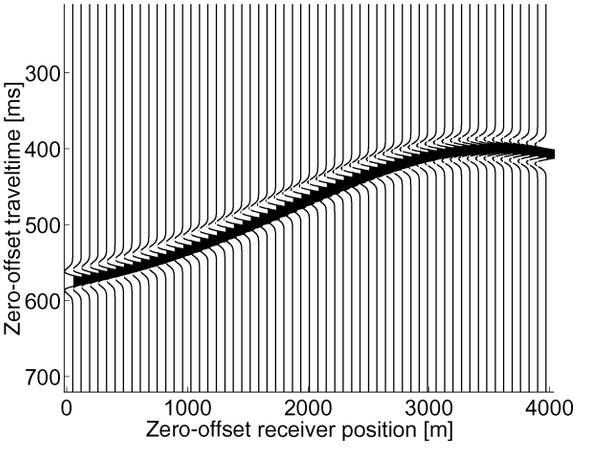

Figure 7. Synthetic zero-offset section for the model in Figure 2.

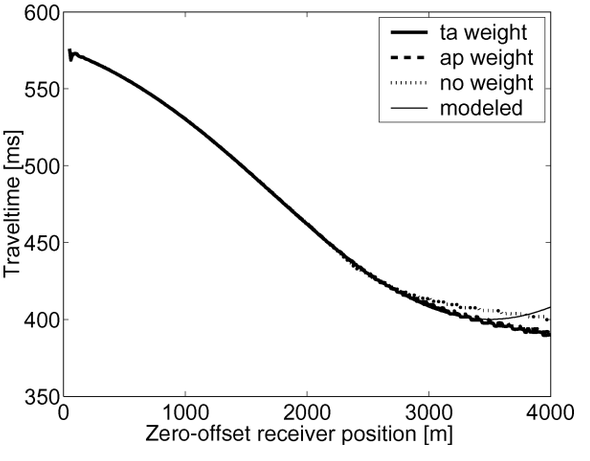

Figure 8. Picked traveltimes of the simulated and modeled zero-offset reflections of Figures 4–7. True-amplitude (ta) simulation: bold line; amplitude-preserving (ap) simulation: dashed line; unweighted simulation: dotted line; modeled traveltimes: thin line.

Kirchhoff CS-MZO are almost perfect up to about 3000 m. Further away from the source, the input data are insufficient to correctly simulate zero-offset traces. However, the weighted CS-MZO schemes produce correct traveltimes for slightly larger offsets than the unweighted version. The most probable reason is the interference of the strong boundary effect of unweighted CS-MZO (see Figure 6) with the simulated zero-offset event. This observation can be confirmed in Figure 9, which depicts the relative error of the traveltimes as compared to the modeled zero-offset reflections of Figure 7. Where the data coverage is sufficient, the error is of the order of 0.1%.

The quality of the amplitudes along the simulated zero-offset reflections of Figures 4–6 is discussed with the help of the next figures. Figure 10 compares the amplitudes obtained with a true-amplitude CS-MZO to those of the modeled section. The amplitudes are quite well recovered within the region between about 300 and 2100 m, which is not affected by boundary effects.

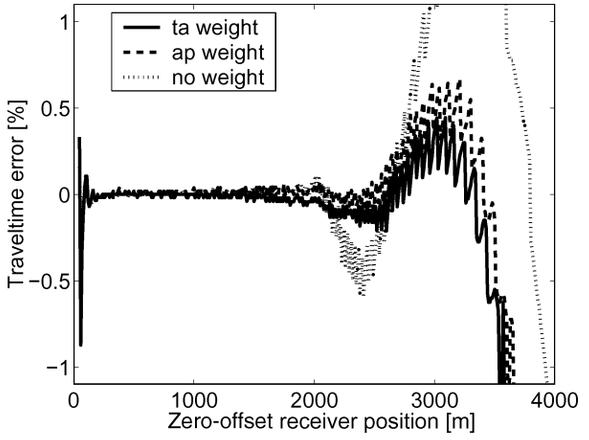

Figure 9. Traveltime error of the simulated zero-offset reflections as compared to the modeled ones. True-amplitude (ta) simulation: bold line; amplitude-preserving (ap) simulation: dashed line; unweighted simulation: dotted line.

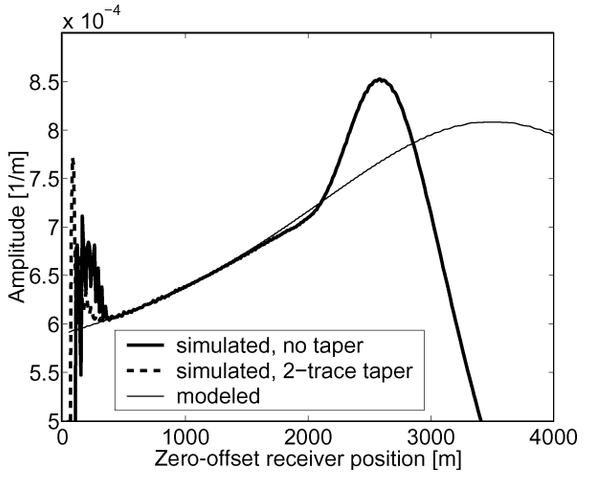

Figure 10. Picked amplitudes of the simulated zero-offset reflections resulting from a true-amplitude CS-MZO with (dashed line) and without (bold line) a two-trace taper, together with the modeled amplitudes (thin line).

Within this region, the amplitude error is less than 1%, as can be seen in Figure 11. The size of left boundary region can be reduced by a two-trace taper function (dashed line). Larger tapers did not improve the quality of the result but produced stronger precursors. The boundary effects are discussed further below.

Figure 12 shows the amplitudes obtained with the amplitude preserving CS-MZO, together with the desired result, which in this case is just a unit amplitude. Except for the boundary regions, the amplitude preservation works quite well even though the reflector is curved. The amplitude error is depicted in Figure 13. Because of the curved reflector, the error is slightly larger than that of true-amplitude CS-MZO (see Figure 11) at about 2%. The amplitude error will increase as the curvature of the target reflector increases. This can only be avoided by using the correct curvature dependence for the geometrical-spreading correction, which is impossible in practice since the reflector curvature is unknown at this stage. Therefore, the

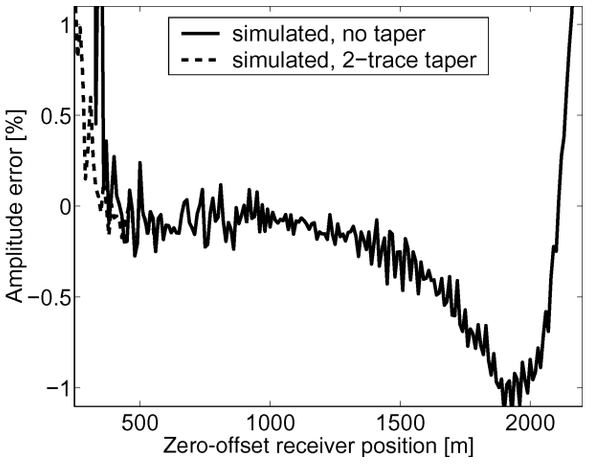

Figure 11. Amplitude error of the true-amplitude CS-MZO reflections as compared to the modeled ones.

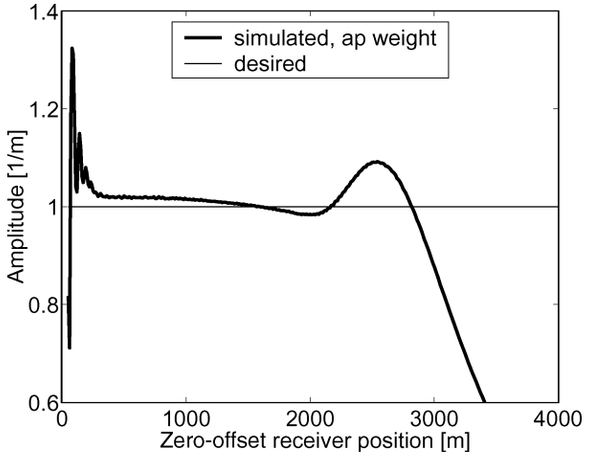

Figure 12. Picked amplitudes of the simulated zero-offset reflections resulting from an amplitude-preserving CS-MZO (bold line), together with the desired unit amplitude (thin line).

spreading correction is generally realized by simply scaling the traces with traveltime (and velocity) as simulated in this example.

For comparison, Figure 14 shows the amplitudes after an unweighted CS-MZO. Consistent with Hearn (1989), we observe that unweighted CS-MZO amplitudes increase with increasing distance from the original source. Moreover, not only the shape of the curve is different from the desired one (see Figure 12), but also the scale is completely wrong.

Finally, Figure 15 shows the amplitudes as obtained with Hearn's (1989) weight. Note that these amplitudes are much better than the ones obtained from an unweighted CS-MZO (compare to Figure 14), but still remain about 40% below the desired unit amplitude.

Figure 16 is a graphical explanation of the edge effects in Figure 10 due to the aperture (equation 8) of the Kirchhoff-type stack in equation 1. Four stacking lines (equation 6), corresponding to four different zero-offset locations s_0, are depicted. The black ends of the stacking lines indicate the taper region. We see that very close to the original source, the stacking operator is very small. In this region, the stack 1 does not achieve any interference. Thus, the simulated zero-offset reflections are plain wrong. Very far from the original source, the stacking operator follows exactly the common-shot reflections, and would do so well beyond the data boundary. For a complete simulation, data beyond the boundary are missing. Only inside an intermediate region, the operator is large enough to achieve complete interference, but its end point does not fall into the original reflection. It is inside this region that a true-amplitude or amplitude-preserving CS-MZO will work.

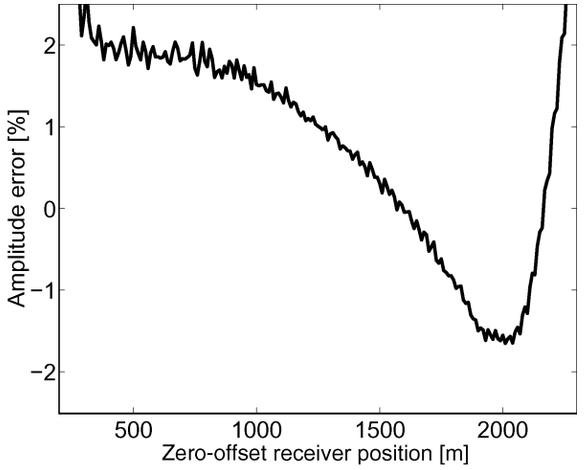

Figure 13. Amplitude error of the amplitude-preserving CS-MZO reflections as compared to the desired unit amplitude.

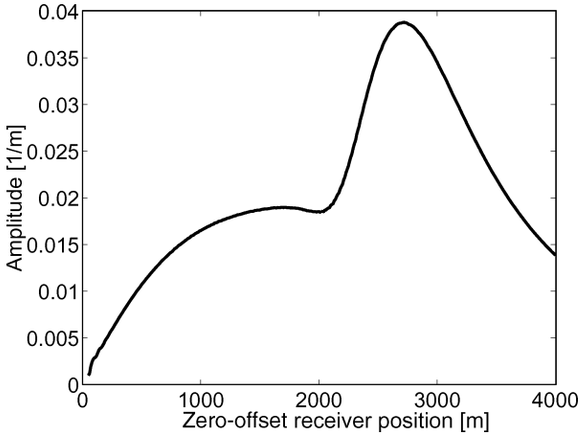

Figure 14. Picked amplitudes of the simulated zero-offset reflections resulting from an unweighted CS-MZO.

CONCLUSIONS

In this paper, we have formulated a new Kirchhoff-type approach to amplitude controlled common-shot migration to zero offset (CS-MZO) for 2.5D in-plane reflections in 2D laterally inhomogeneous media with curved interfaces. We have presented the weight functions for amplitude-preserving and true-amplitude CS-MZO. Here, to preserve CS-MZO

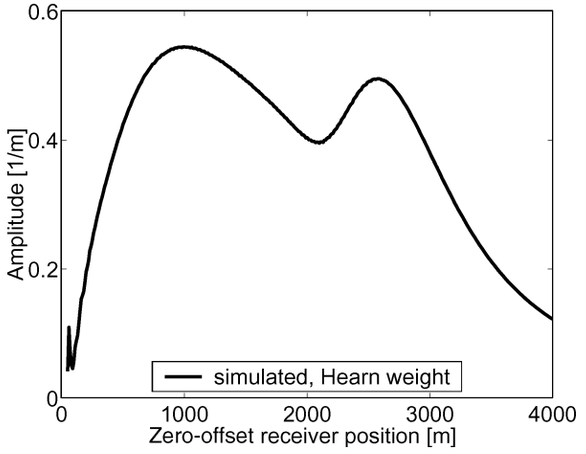

Figure 15. Picked amplitudes of the simulated zero-offset reflections resulting from a CS-MZO with Hearn's (1989) weight (corrected for the application as an MZO rather than DMO).

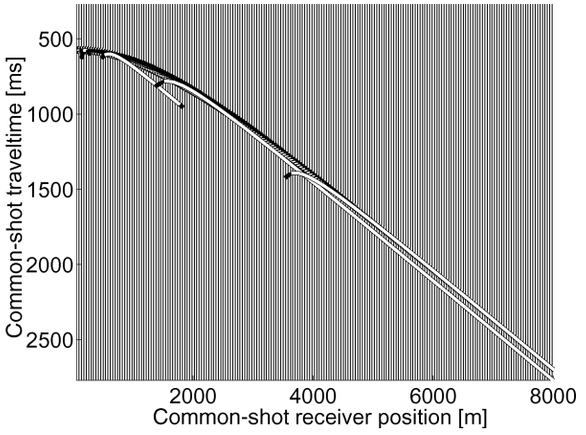

Figure 16. Stacking operators for four different output points (white lines) overlaid on the input common-shot data. The black tips of the operators correspond to the size of the two-trace taper. At small offsets, the operator is too small to achieve interference, while at large offsets, the data aperture is to small.

amplitudes means that output amplitudes are equal to input amplitudes, while to construct true CS-MZO amplitudes implies that, in a simulated zero-offset reflection, the geometrical-spreading factor of the original common-shot reflection is replaced by the new zero-offset one for the same reflection point. This goal is achieved by a weighted one-fold single-stack integral in the time domain along specific stacking lines, the inplanats. We stress that the true-amplitude weight does not rely on any prior knowledge about the arbitrarily curved reflectors to be imaged and is theoretically valid for any reflector curvature, while the amplitude-preserving weight is strictly valid for planar reflectors only. Both, the true-amplitude and the amplitude-preserving weight functions can be computed, for instance, by 2D dynamic ray tracing performed along ray segments that link the two common-offset pairs of source and receivers to certain points in the macrovelocity model.

First numerical results show that true-amplitude and amplitude-preserving CS-MZO can be realized with sufficient accuracy. In this way, zero-offset sections can be simulated directly from shot records as an alternative to the standard NMO/DMO procedure that relies on common-offset data.

ACKNOWLEDGMENTS

We are grateful to Sergey Fomel and two anonymous reviewers for their constructive remarks. The research of this paper has been supported partially by the Research Foundation of the State of São Paulo (FAPESP), the National Research Council (CNPq) of Brazil, and the sponsors of the WIT Consortium Project.

APPENDIX A

CONSTANT-VELOCITY MEDIUM

In this appendix, we derive the expressions 6 and 12 for the CS-MZO stacking line and weight function in a constant-velocity medium.

CS-MZO stacking line in a constant velocity medium

A point (s_0, t_0) in the output section determines in the image space $z > 0$ the isochron $z = \mathcal{Z}_{ZO}(x; s_0, t_0)$, implicitly defined by equation 3. For a constant velocity v, equation 3 can be solved for z to yield

$$z = \mathcal{Z}_{ZO}(x; s_0, t_0) = \sqrt{R_0^2 - (x - s_0)^2}, \tag{A-1}$$

which is a half-circle with radius $R_0 = vt_0/2$ (see Figure 1).

Therefore, the diffraction traveltime $\mathcal{T}_D(x; s, h)$, which is the sum of the traveltimes along the (straight-line) ray segments from S to an arbitrary point M on the above isochron A-1, i.e., $M = (x, \mathcal{Z}_{ZO}(x; s_0, t_0))$ and from M to G, can be recast as

$$\mathcal{T}_D(x; s, h) = \frac{R_S + R_G}{v}, \tag{A-2}$$

where

$$R_S = \sqrt{(x - s)^2 + R_0^2 - (x - s_0)^2} \tag{A-3}$$

and

$$R_G = \sqrt{(x - s - 2h)^2 + R_0^2 - (x - s_0)^2} \tag{A-4}$$

are the distances from M to S and G, respectively.

Upon the introduction of relative coordinates $X = x - s$ and $\eta = s_0 - s$, equation A-2 can be recast into the form

$$\mathcal{T}_D(x; s, h) = \frac{1}{v}\sqrt{R_0^2 + 2\eta X - \eta^2} + \frac{1}{v}\sqrt{R_0^2 + 2(\eta - 2h)X + 4h^2 - \eta^2}. \tag{A-5}$$

Applying the stationary condition 5 to equation A-5, we find

$$\left.\frac{\partial \mathcal{T}_D}{\partial X}\right|_{X^*} = \frac{1}{v}\frac{\eta}{\sqrt{R_0^2 + 2\eta X^* - \eta^2}} + \frac{1}{v}\frac{\eta - 2h}{\sqrt{R_0^2 + 2(\eta - 2h)X^* + 4h^2 - \eta^2}} = 0. \tag{A-6}$$

From this equation, it is obvious that there can be only a stationary point if the two terms have opposite sign. Since the denominators are always positive, it follows that for positive η, $\eta - 2h < 0$ or $h > \eta/2$, and for negative η, $\eta - 2h > 0$ or $h < \eta/2$. In other words, to construct a zero-offset trace at s_0, only traces will be needed that are recorded at receivers on the same side of s as s_0 and further away from s than s_0. Since the axis can always be chosen accordingly, we restrict our further analysis to positive η and h.

Solving equation A-6 for X^*, we find the stationary point at

$$X^*(h; s_0, t_0) = \eta - R_0^2\frac{h - \eta}{\eta(2h - \eta)} = \eta + (\eta - h)\rho, \tag{A-7}$$

where we have introduced the notation

$$\rho = \frac{R_0^2}{\eta(2h - \eta)}. \tag{A-8}$$

Substituting this result in equations A-3 and A-4 yields, after some algebraic manipulations,

$$R_S^* = \sqrt{\eta^2(1 + \rho)} = \eta\sqrt{1 + \rho}, \tag{A-9}$$

$$R_G^* = \sqrt{(2h - \eta)^2(1 + \rho)} = (2h - \eta)\sqrt{1 + \rho}, \tag{A-10}$$

where we have used that $\eta > 0$ and $2h > \eta$, as observed in connection with equation A-6. With this expressions, the traveltime A-2 is

$$\begin{aligned}\mathcal{T}(h; s_0, t_0) &= \mathcal{T}_D(x^*; s, h) = \mathcal{T}_D(X^*; \eta, h)\\ &= \frac{1}{v}(\eta + (2h - \eta))\sqrt{1 + \rho}\\ &= \frac{2h}{v}\sqrt{1 + \rho},\end{aligned} \tag{A-11}$$

which is the expression for $\mathcal{T}$ indicated in equation 6.

Aperture consideration

To determine the aperture A to be used in stack 1, we use the condition that the stationary point X^* as given by equation A-7 must be located on the real extension of the zero-offset isochron A-1. This translates into the mathematical restriction

$$\eta - R_0 < X^* < \eta + R_0. \tag{A-12}$$

Substitution of equation A-7 leads to the condition

$$-1 < R_0 \frac{h-\eta}{\eta(2h-\eta)} < 1, \tag{A-13}$$

which, because of the above observation that $\eta > 0$ and $2h - \eta > 0$, reduces to

$$R_0|h-\eta| < \eta(2h-\eta). \tag{A-14}$$

Here, we must distinguish two cases:

1) For $h \geq \eta$, condition A-14 yields

$$(R_0 - 2\eta)h < \eta(R_0 - \eta), \tag{A-15}$$

which is always satisfied for $R_0 = 2\eta$ and for other values of R_0 leads to the following conditions on h:

$$\begin{aligned} h &< \frac{\eta(R_0-\eta)}{R_0-2\eta} \quad \text{for} \quad R_0 > 2\eta, \\ h &> \frac{\eta(R_0-\eta)}{R_0-2\eta} \quad \text{for} \quad R_0 < 2\eta. \end{aligned} \tag{A-16}$$

Since

$$\frac{\eta(R_0-\eta)}{R_0-2\eta} = \eta + \frac{\eta^2}{R_0-2\eta} \begin{cases} > \eta & \text{for} \quad R_0 > 2\eta \\ < \eta & \text{for} \quad R_0 < 2\eta, \end{cases} \tag{A-17}$$

the original condition A-14 is satisfied in case 1 if

$$\begin{aligned} \eta \leq h &< \frac{\eta(R_0-\eta)}{R_0-2\eta} \quad \text{for} \quad R_0 > 2\eta \\ \eta \leq h &< \infty \quad \text{for} \quad R_0 \leq 2\eta. \end{aligned} \tag{A-18}$$

2) For $h < \eta$, condition A-14 yields

$$-(R_0 + 2\eta)h < -(R_0 + \eta)\eta. \tag{A-19}$$

Since R_0 and η are positive, the resulting condition for h is

$$h > \frac{\eta(R_0+\eta)}{R_0+2\eta}. \tag{A-20}$$

The condition that h must be larger than $\eta/2$ is implicitly satisfied by inequality A-20. The combination of results A-18 and A-20 yields the aperture condition as stated in equation 8.

CS-MZO weight function in a constant-velocity medium

To derive the constant-velocity weight function 12 from its general 2.5D representation 9, we start by discussing several geometric features that are specific to constant-velocity CS-MZO.

Curvatures of the isochrons.—The isochron of the zero-offset configuration is given by equation A-1; that of the common-shot configurations is a half-ellipse with the form

$$z = \mathcal{Z}_{CS}(x; s, h) = b\sqrt{1 - \frac{(x-s-h)^2}{a^2}}, \tag{A-21}$$

where $a = v\mathcal{T}/2$ and $b = \sqrt{a^2 - h^2}$ are the semiaxes. Therefore, we conclude from equation A-11 that

$$a = h\sqrt{1+\rho} \quad \text{and} \quad b = h\sqrt{\rho}. \tag{A-22}$$

The curvatures K_0 and K of the isochrons A-1 and A-21 at a point $M = (x, z)$ are given by

$$K_0 = \frac{d^2\mathcal{Z}_{ZO}/dx^2}{[1 + (d\mathcal{Z}_{ZO}/dx)^2]^{3/2}} = -\frac{1}{R_0} \tag{A-23}$$

and

$$\begin{aligned} K &= \frac{d^2\mathcal{Z}_{CS}/dx^2}{[1 + (d\mathcal{Z}_{CS}/dx)^2]^{3/2}} \\ &= -\frac{b}{a^2}\left(1 - \frac{h^2(x-s-h)^2}{a^4}\right)^{-3/2}, \end{aligned} \tag{A-24}$$

respectively. In particular, at the stationary point M^*, we have

$$K = -\frac{h^2}{R_0^3}\frac{\rho^2}{1+\rho}. \tag{A-25}$$

In the formula for the weight function, we need the curvature difference $K - K_0$:

$$\begin{aligned} K - K_0 &= -\frac{h^2}{R_0^3}\frac{\rho^2}{1+\rho} - \frac{-1}{R_0} \\ &= \frac{1}{R_0}\left[1 - \frac{h^2}{R_0^2}\frac{\rho^2}{1+\rho}\right]. \end{aligned} \tag{A-26}$$

Reflection angles.—Another quantity that enters into the computation of the weight function 9 is the reflection angle θ. To compute it, we use the well-known law of cosines (see Figure 1),

$$\begin{aligned} (2h)^2 &= \left(R_S^*\right)^2 + \left(R_G^*\right)^2 - 2R_S^*R_G^*\cos 2\theta \\ &= \left(R_S^* + R_G^*\right)^2 - 4R_S^*R_G^*\cos^2\theta, \end{aligned} \tag{A-27}$$

where R_S^* and R_G^* are given by equations A-9 and A-10. Therefore,

$$\cos^2\theta = \frac{4h^2 - \left(R_S^* + R_G^*\right)^2}{-4R_S^*R_G^*} = \frac{h^2}{R_0^2}\frac{\rho^2}{1+\rho}. \tag{A-28}$$

Using this expression in equation A-26, we can verify that

$$K - K_0 = \frac{1}{R_0}[1 - \cos^2\theta] = \frac{\sin^2\theta}{R_0}, \tag{A-29}$$

which implies that $\mathrm{sgn}(K - K_0) = 1$. Thus, the last factor in weight 9 becomes

$$\exp\left\{i\frac{\pi}{2}\kappa\right\} = \exp\left\{i\frac{\pi}{4}[1 - \mathrm{sign}(K - K_0)]\right\} = 1. \tag{A-30}$$

Beylkin's determinant.—We consider the 2D Beylkin determinant

$$h_B = \det\begin{pmatrix} \dfrac{\partial}{\partial x}\mathcal{T}_D(x,z;h) & \dfrac{\partial}{\partial z}\mathcal{T}_D(x,z;h) \\ \dfrac{\partial^2}{\partial x\partial h}\mathcal{T}_D(x,z;h) & \dfrac{\partial^2}{\partial z\partial h}\mathcal{T}_D(x,z;h) \end{pmatrix}, \tag{A-31}$$

where

$$\mathcal{T}_D(x,z;h) = \frac{1}{v}\sqrt{(x-s)^2 + z^2} + \frac{1}{v}\sqrt{(x-s-2h)^2 + z^2}. \tag{A-32}$$

All these quantities are taken at the stationary point $M^* = (x^*, z^*)$ with

$$z^* = \mathcal{Z}_{CS}(x^*; h, t) = \mathcal{Z}_{ZO}(x^*; s_0, t_0) = \sqrt{R_0^2(1+\rho) - h^2\rho^2}. \quad \text{(A-33)}$$

With the help of the stationary value A-7 and the formulas A-9 and A-10 for R_S^* and R_G^*, determinant A-31 reduces to

$$|h_B| = \frac{4h^2\rho\sqrt{R_0^2(1+\rho) - h^2\rho^2}}{v^2(2h-\eta)^3\eta(1+\rho)^2}. \quad \text{(A-34)}$$

Combining equations A-26, A-30, and A-34, we find for the last factors in equation 9

$$\frac{|h_B|}{\sqrt{|K-K_0|}} \exp\left\{i\frac{\pi}{2}\kappa\right\} = \frac{\dfrac{4h^2\rho\sqrt{R_0^2(1+\rho) - h^2\rho^2}}{v^2(2h-\eta)^3\eta(1+\rho)^2}}{\sqrt{\dfrac{R_0^2(1+\rho) - h^2\rho^2}{R_0\, R_0^2(1+\rho)}}} \cdot 1$$

$$= \frac{4h^2\rho^2}{v^2(2h-\eta)^2(1+\rho)^{3/2}\sqrt{R_0}}. \quad \text{(A-35)}$$

Out-of-plane Fresnel factors.—In a constant-velocity medium, the out-of-plane Fresnel factors $\mathcal{L}_F$ and $\mathcal{L}_{F0}$ have the simple forms

$$\mathcal{L}_F = \left(\frac{1}{vR_S^*} + \frac{1}{vR_G^*}\right)^{-1/2} = (1+\rho)^{1/4}\sqrt{\frac{v\eta(2h-\eta)}{2h}} \quad \text{(A-36)}$$

and

$$\mathcal{L}_{F0} = \left(\frac{1}{vR_0} + \frac{1}{vR_0}\right)^{-1/2} = \sqrt{\frac{vR_0}{2}}. \quad \text{(A-37)}$$

Point-source geometrical spreading factors.—The geometrical spreading factors are just the distances from the source or receiver. In other words, $\mathcal{L}_0 = R_0$, $\mathcal{L}_S = R_S^*$, and $\mathcal{L}_G = R_G^*$. Therefore, the spreading term in weight 9 reduces to

$$\frac{\mathcal{L}_S\mathcal{L}_G}{\mathcal{L}_0^2}\frac{\mathcal{L}_{F0}}{\mathcal{L}_F} = (1+\rho)^{3/4}\sqrt{\frac{h}{R_0\rho}}. \quad \text{(A-38)}$$

Final weight function.—We are now in the position of actually computing the weight function $\mathcal{W}^{TA}(h; s_0, t_0)$ for a constant velocity medium. Substituting the above intermediate results A-28, A-35, and A-38 in equation 9, we finally arrive at

$$\mathcal{W}^{TA}(h; s_0, t_0) = \left(\frac{v}{2}\right)^{3/2}(1+\rho)^{3/4}\sqrt{\frac{h}{R_0\rho}}\frac{R_0^2(1+\rho)}{h^2\rho^2} \times \frac{4h^2\rho^2}{v^2(2h-\eta)^2(1+\rho)^{3/2}\sqrt{R_0}}$$

$$= \sqrt{\frac{2h}{v}\sqrt{1+\rho}}\frac{R_0}{\sqrt{\rho}}\frac{1}{(2h-\eta)^2}. \quad \text{(A-39)}$$

Under the first square root, we recognize $\mathcal{T}$ as given in equation A-11. Upon the use of equation A-8, the weight function A-39 can then be recast into the form of equation 12.

REFERENCES

Bagaini, C., and U. Spagnolini, 1996, 2D continuation operators and their applications: Geophysics, **61**, 1846–1858.

Beylkin, G., 1985, Imaging of discontinuities in the inverse scattering problem by inversion of a generalized Radon transform: Journal of Mathematical Physics, **26**, 99–108.

Biondi, B., S. Fomel, and N. Chemingui, 1998, Azimuth moveout for 3-D prestack imaging: Geophysics, **63**, 574–588.

Biondi, B., and J. Ronen, 1987, Dip moveout in shot profiles: Geophysics, **52**, 1473–1482.

Black, J. L., K. L. Schleicher, and L. Zhang, 1993, True-amplitude imaging and dip moveout: Geophysics, **58**, 47–66.

Bleistein, N., 1986, Two-and-one-half dimensional in-plane wave propagation: Geophysical Prospecting, **34**, 686–703.

——— 1987, On the imaging of reflectors in the earth: Geophysics, **52**, 931–942.

Bleistein, N., and J. K. Cohen, 1995, The effect of curvature on true-amplitude DMO: Proof of concept: Research Note, Center for Wave Phenomena, **CWP-193**.

Bleistein, N., J. K. Cohen, and F. G. Hagin, 1987, Two and one-half dimensional Born inversion with an arbitrary reference: Geophysics, **52**, 26–36.

Bleistein, N., J. K. Cohen, and H. Jaramillo, 1999, True-amplitude transformation to zero offset of data from curved reflectors: Geophysics, **64**, 112–129.

Cabrera, J., and S. Levy, 1989, Shot dip moveout with logarithmic transformations: Geophysics, **54**, 1038–1041.

Canning, A., and G. H. F. Gardner, 1996, Regularizing 3D data sets with DMO: Geophysics, **61**, 1101–1114.

Červený, V., 1987, Ray methods for three-dimensional seismic modelling, Norwegian Institute for Technology Petroleum Industry Course.

Collins, C. L., 1997, Imaging in 3D DMO; Part I: Geometrical optics model; Part II: Amplitude effects: Geophysics, **61**, 211–244.

Fomel, S., 2003, Theory of differential offset continuation: Geophysics, **68**, 718–732.

Fomel, S., and N. Bleistein, 2001, Amplitude preservation for offset continuation: Confirmation for Kirchhoff data: Journal of Seismic Exploration, **10**, 121–130.

Fomel, S. B., 1994, Kinematically equivalent differential operator for offset continuation of reflected wave seismograms: Russian Geology and Geophysics, **35**, no. 9, 122–134.

Goldin, S. V., and S. B. Fomel, 1995, Estimation of reflection coefficients in DMO: Russian Geology and Geophysics, **36**, no. 4, 103–115.

Granser, H., 1994, Shot gather DMO in the double log domain: Geophysics, **59**, 1305–1307.

Hearn, T. M., 1989, Time domain application of dip moveout to shot gather: 59th Annual International Meeting, SEG, Expanded Abstracts, 1140–1143.

Hubral, P., J. Schleicher, and M. Tygel, 1996, A unified approach to 3-D seismic reflection imaging—Part I: Basic concepts: Geophysics, **61**, 742–758.

Hubral, P., M. Tygel, and H. Zien, 1991, Three-dimensional true-amplitude zero-offset migration: Geophysics, **56**, 18–26.

Jaramillo, H., J. Schleicher, and M. Tygel, 1998, Discussion and errata to: "A unified approach to 3-D seismic reflection imaging, Part II: Theory" (Geophysics, **61**, 759–775, 1996): Geophysics, **63**, 670–673.

Martins, J. L., J. Schleicher, M. Tygel, and L. T. Santos, 1997, 2.5-D true-amplitude Kirchhoff migration and demigration: Journal of Seismic Exploration, **6**, 159–180.

Newman, P., 1975, Amplitude and phase properties of a digital migration process: 37th Annual International Meeting, European Association of Exploration Geophysicists (republished in First Break, **8**, 397–403, 1990).

Santos, L. T., J. Schleicher, and M. Tygel, 1997, 2.5-D true-amplitude offset continuation: Journal of Seismic Exploration, **6**, 103–116.

Schleicher, J., M. Tygel, and P. Hubral, 1993, 3-D true-amplitude finite-offset migration: Geophysics, **58**, 1112–1126.

Tygel, M., J. Schleicher, and P. Hubral, 1994, Kirchhoff-Helmholtz theory in modelling and migration: Journal of Seismic Exploration, **3**, 203–214.

——— 1995, Dualities between reflectors and reflection-time surfaces: Journal of Seismic Exploration, **4**, 123–150.

——— 1996, A unified approach to 3-D seismic reflection imaging—Part II: Theory: Geophysics, **61**, 759–775 [errata in Jaramillo et al. (1998)].

Tygel, M., J. Schleicher, P. Hubral, and L. T. Santos, 1998, 2.5-D true-amplitude Kirchhoff migration to zero offset in laterally inhomogeneous media: Geophysics, **63**, 557–573.